Ultrasound-Based Robot-Assisted Drilling for Minimally Invasive Pedicle Screw Placement

Ruixuan Li, Ayoob Davoodi, Maikel Timmermans, Kaat Van Assche, Orçun Taylan, Lennart Scheys, Matthias Tummers, Gianni Borghesan, Emmanuel Vander Poorten

▶ **To cite this version:**

Ruixuan Li, Ayoob Davoodi, Maikel Timmermans, Kaat Van Assche, Orçun Taylan, et al.. Ultrasound-Based Robot-Assisted Drilling for Minimally Invasive Pedicle Screw Placement. IEEE Transactions on Medical Robotics and Bionics, In press. hal-04514013v2

HAL Id: hal-04514013
https://hal.science/hal-04514013v2

Submitted on 29 Mar 2024

HAL is a multi-disciplinary open access archive for the deposit and dissemination of scientific research documents, whether they are published or not. The documents may come from teaching and research institutions in France or abroad, or from public or private research centers.

L'archive ouverte pluridisciplinaire **HAL**, est destinée au dépôt et à la diffusion de documents scientifiques de niveau recherche, publiés ou non, émanant des établissements d'enseignement et de recherche français ou étrangers, des laboratoires publics ou privés.

Ultrasound-Based Robot-Assisted Drilling for Minimally Invasive Pedicle Screw Placement

Ruixuan Li*, Ayoob Davoodi*, Maikel Timmermans, Kaat Van Assche, Orçun Taylan, Lennart Scheys, Matthias Tummers, Gianni Borghesan, and Emmanuel Vander Poorten

***Abstract*—Minimally invasive pedicle screw placement (MIPSP) is a widely used treatment for spine diseases. When coupled with intraoperative navigation modalities, robots may help improve surgical outcomes and reduce complications. With such a system, the application of pedicle screws has been expanded from needle insertion to the spine surgery. This paper investigates the possibility and feasibility of robot-assisted MIPSP based on ultrasound (US) guidance. The proposed system is non-radiative and fiducial-free, using purely image information to close the registration loop. Then the system automatically positions the drill tip to a planned screw trajectory and executes the drilling operation. Experiments were conducted on both ex-vivo lamb and human cadaver spines. An entry point accuracy of 2.39 ± 1.41 mm, and orientation accuracy of $2.82 \pm 1.85°$ was found for 24 drilled trajectories on three lamb spines. On the ex-vivo human spine, the position error averaged 3.08 ± 2.43 mm at the entry point and 4.05 ± 2.62 mm at the stop point across 16 drilling instances. Moreover, a 87.5% success rate was reported by using Gertzbein-Robbins grade. The experimental results demonstrate the potential for offering a radiation-free alternative. Although restricted to cadaver trials, this work encourages further exploration of this technology to assist surgeons in maximizing performance in clinical practice.**

***Index Terms*—3D reconstruction, pedicle screw placement, robot-assisted system, ultrasound navigation**

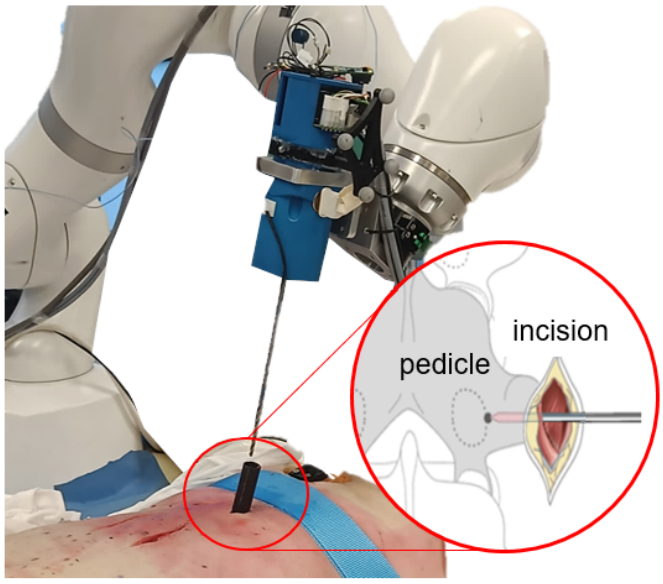

Fig. 1. A demonstration of minimally invasive pedicle screw placement with a robot-assisted system.

I. Introduction

Minimally invasive pedicle screw placement (MIPSP) is a common step for posterior fixation in spinal surgery because of its biomechanical superiority and ability to offer significant corrections to the spine [1]. It also leads to reduced revision rates, lower infection rates, shorter hospital stays, and considerable economic benefits compared to the non-minimally invasive case. However, MIPSP still faces challenges such as limited visibility and poor tissue discrimination. Inaccurate pedicle screw placement (PSP) may lead to neurological impairment such as pain, weakness or sensory loss. Screw placement is an error-prone and time-consuming step of MIPSP when performed manually [2]. Great care needs to be demonstrated in this procedure, as screw placement accuracy is paramount and critical for a successful surgery [3].

Computer-assisted techniques, such as fluoroscopy, have already been developed for assisting screw positioning, insertion and evaluation. Applied to the lumbar spine, 3D navigated PSP has been shown to significantly improve screw accuracy up to 97.5% [4]. However, cumulative radiation exposure from fluoroscopic imaging can pose risks to surgeons, surgical staff and patients over time [5]. It is crucial to investigate non-radiative intraoperative navigation technologies providing cross-sectional and 3D images of anatomy.

Ultrasound (US) imaging offers an alternative to fluoroscopy due to its non-invasive nature and ability to visualize hidden anatomic structures [6]. However, high-quality free-hand US examination requires surgeons' substantial experience and visuo-tactile skills. Robot-assisted US systems could offer even better reproducibility, improve dexterity, and may also offer better image quality [7]. Contrary to computer-assisted applications that are already part of the standard of PSP, the development of US-based robotics in spine surgery is still in its infancy and not used in clinical practice. Thus, it is important to investigate a combination of US imaging and robotics system to effectively guide the placement of pedicle screws.

* These authors contributed equally to this work.

This project has received funding from the European Union's Horizon 2020 research and innovation program under grant agreement NO.101016985 (FAROS) and Flemish Research Foundation (FWO) under grant agreement NO.G0A1420N, NO.1S36324N, NO.1S35424N, and NO.1SHGA24N. Ethical approval No.NH019 2022-1-02 was granted by the Belgian National Council for Bioethics.

Ruixuan Li, Ayoob Davoodi, Maikel Timmermans, Kaat Van Assche, Matthias Tummers, and Emmanuel Vander Poorten are with the Robot-Assisted Surgery (RAS) group, KU Leuven, Belgium. (ruixuan.li@kuleuven.be)

Gianni Borghesan is with Robot-Assisted Surgery (RAS) group, KU Leuven, Belgium, and also with Flanders Make@KU Leuven, Leuven, Belgium.

Orçun Taylan and Lennart Scheys are with the Institute for Orthopaedic Research and Training (IORT), Development and Regeneration Department, KU Leuven, Belgium.

Previous studies found that a key issue in accurate screw placement is the surgeon's ability to maintain the correct position and angle of the instrument at the entry point [8]. Thus, it is important to perform the drilling procedure with the assistance of a robotic system, following the screw trajectory from computer-assisted navigation. Recently, such robotic drilling systems have already demonstrated efficacy in guiding drill bits with precision and accuracy [9]. For example, in the work by Jiang *et* al., the robot serves primarily as a guide for the drill bit throughout the operation, while the surgeon retains manual control of the procedure. Thus, the combination of the robot, US imaging system and drilling system is important. It is the key to closing the gap in the flow of information between surgical planning and procedure execution.

To the best of our knowledge, there is no work demonstrating the feasibility of robot-assisted PSP while excluding radiological imaging or an external tracking system. Thus, this paper proposes a radiation-free robotic system for MIPSP. The system utilizes a neural network to segment US images and then reconstruct the spine structure in 3D space. A computed tomography (CT) to US registration algorithm is employed to transform the preoperative surgical plan into the US reconstruction model. The robot then automatically guides the drilling procedure, which controls the drilling force.

The contributions of the work are listed as follows:

- investigation and validation of the feasibility of robot-assisted MIPSP procedures under US navigation.
- development of US-based method to register the preoperative CT.
- implementation of a robotic drilling system for screw placement.
- experimental validation using ex-vivo lamb and human spines demonstrating the performance of the proposed system, indicating its potential for clinical use.

The rest of the paper is organized as follows. Section II discusses the state-of-the-art in US navigation and robotic drilling systems. Section III presents the implementation details of the navigation and drilling system. Then, the experimental setup and ex-vivo cadaver spines are described in Section IV. Section V describes the experimental results. Finally, the discussion and conclusion are given in Sections VI and VII, respectively.

II. Related Work

In this section, the surgical procedure is described. Then, related works on intraoperative navigation and robot-assisted drilling system are discussed.

A. Surgical Approach

With manual MIPSP, the spinous processes are localized through palpation and verified by a navigation system such as fluoroscopy. Then, a small incision is manually made using a scalpel by opening the fascia on the right and left side [10]. Dilators are inserted into the incision along a predefined trajectory to separate the muscle tissue until the cannulated bone surface [11], as shown in Fig.2. Subsequently, the surgeon verifies the drill bit position by using fluoroscopy. Subsequently, the surgeon drills through the pedicle. Meanwhile, an assistant holds the dilator, maintaining the drill orientation. After drilling, a ball-tip probe is used to evaluate the integrity of the cortical walls within the vertebra and detect any breaches. Then, the screw is inserted. This happens by using guided instruments such as Kirchner wires (K-wire). This sequence is repeated until all pedicles are drilled. Finally, intraoperative fluoroscopy images are acquired to verify the correctness of the screw and rod position.

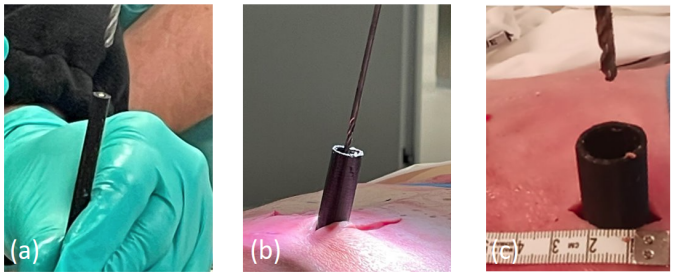

Fig. 2. (a) and (b) show dilators with different diameters used in MIPSP. (c) Illustration of the dimension of the incision with the largest dilator.

B. Intraoperative Navigation

Intraoperative navigation systems, such as fluoroscopy, are necessary for accurate PSP to visualize anatomic features and confirm accurate placement. Several commercial systems have been developed. The Mazor Renaissance (Medtronic, Dublin, Ireland) is developed to assist screw placement with fluoroscopic images. Registration is applied to the preoperative CT, followed by the guided placement of a particular screw. The drawback of these technologies is that the use of radiative imaging leads to indirect harm to the patient and clinical staff.

To address this issue, alternative navigation techniques have emerged. Approaches employing optical tracking systems are being widely used, showing considerably higher accuracy compared to fluoroscopic guidance [4], [12], [13]. Optical tracking systems are investigated due to their ability to detect the real-time position of the patient [14]. ROSA (Zimmer Biomet, Warsaw, IN) and Excelsius GPS (Globus Medical, Inc., Audubon, PA) offer robotic-assisted PSP with optical navigation [15], [16]. The navigation system provides real-time instrument tracking by registering the optical markers on the patient and on the robot. The original ROSA robot has achieved a 96.3% [17] grades A or B rate by using Gertzbein-Robbin (GR) grade [18]. However, optical systems rely on the line of sight and suffer from occlusion and deformation between markers and drill sites.

US provides a radiation-free alternative for intraoperative navigation. Barbe *et al.* first proposed a US-based intraoperative navigation system for spine surgery [19]. It included an anatomic registration allowing to guide the surgeon towards preoperative surgical planning. Ottacher *et al.* reported a free-hand US approach to reconstruct the 3D vertebra anatomy for PSP, achieving 0.8 ± 0.6 mm position accuracy on synthetic models [20]. This work was manually conducted on a synthetic experiment phantom. Zhang *et al.* utilized a flexible US scanning system to automatically image the human spine [21]. The probe

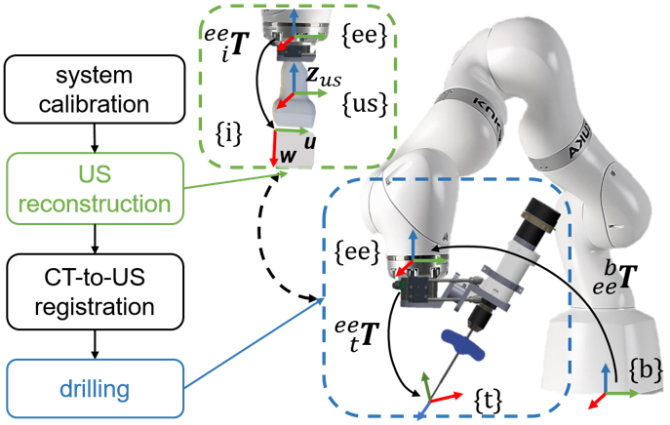

Fig. 3. The workflow of the proposed system. The involved transformations and coordinate frames for the US navigation and drilling system. The transformation ${}^{B}_{A}\boldsymbol{T}$ denotes the frame $\{A\}$ with respect to the frame $\{B\}$.

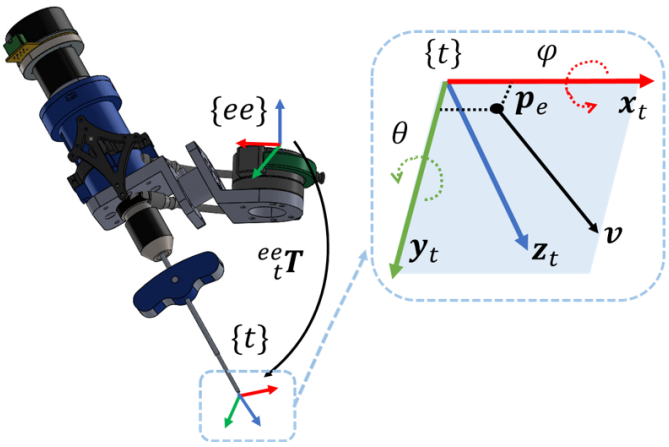

Fig. 4. Illustration of the customer-designed drilling system and the manufacturing error represented in the drill tip frame.

was fixed on a robotic arm with a flexible fixture. Then automatic scanning was conducted with a constant 8 N force. However, the system was only validated on a synthetic phantom with a flat silicon surface. It is important to perform further pre-clinical validation on the robotic US system.

C. Robot-assisted Drilling

The introduction of robotics into spine surgery holds the potential for improved clinical outcomes and patient safety [22]. Li *et al.* performed a meta-analysis that shows that robot-assisted system interventions achieved an 88.9% grade A according to the GR classification, compared to 84.0% for freehand screw placement [23]. Additionally, the learning curve for robot-assisted PSP is reported to be significantly shorter than that of the manual technique [24].

Several studies have been proposed to assist PSP with computer-assisted robotic systems [25], [26]. Ortmaier *et al.* developed a hands-on-robot system with optical navigation to perform screw placement [25]. Similarly, Tian *et al.* proposed an optical camera based robotic system to recognize the drilling state automatically. It combined the pre-operative surgical plan with force signals to sense the different operation states and to prevent potential cortical penetration [27]. Smith *et al.* also implemented a camera-based supervisory controlled robot for automatic polyaxial screw placement in open surgery [26]. The accuracy of the entry point was 0.49 ± 0.17 mm, while that of the destination point was 1.49 ± 0.46 mm compared to the preoperative CT model. However, this system mentioned above relies on palpation of the bone surface using an exchangeable instrument; it is incompatible with minimally invasive surgery (MIS).

Thus, it is crucial to develop a robotic system that could provide accurate screw placement for real clinical practice. However, the development of robotic systems for PSP remains a work in progress, and further research is needed to address the challenges of manual control [28]. This contrasts with autonomous surgery, where the robot performs the task automatically. Moreover, instrument calibration also plays a significant role in determining screw placement accuracy.

III. Method

The proposed system consists of two main components: a robotic US system and a drilling system. The US system is designed to assist robotic drilling. A single robot with a quick tool exchanger carries a US probe and an actuated drill consecutively. The drilling procedure is executed based on the trajectory that is localized via the US reconstruction. A system block diagram is shown in Fig.3. The transformation ${}^{B}_{A}\boldsymbol{T}$ denotes the frame $\{A\}$ with respect to the frame $\{B\}$.

A. System Calibration

To ensure the screw placement accuracy, calibration procedures are performed. The US system and the drilling system are calibrated and registered separately. The procedures are described in Section III-A1 and Section III-A2, respectively.

1) US Images Calibration: The US image calibrations, including temporal and spatial calibration, are performed beforehand with a custom-designed Z phantom, as described in [29]. The temporal calibration compensates for the frameshift offset between the robot and the image time frame. The US spatial calibration is performed to figure out the transformation matrix from the US image frame $\{i\}$ to the robot end effector frame $\{ee\}$ as ${}^{ee}_{i}\boldsymbol{T}$, as well as the scaling factor matrices $\boldsymbol{T}_s$. Figure 3 shows a schematic overview of the different coordinate frames with the relevant transformations used throughout this work. The calibration accuracy is measured to be 1.21 ± 0.91 mm using a custom-designed phantom [29].

2) Drill Tip Registration: Due to the manufacturing error, there is an essential need for the drill tip registration with respect to the robot end effector frame. A CT of the drilling system is segmented initially to extract the exact model of the drilling system. Afterwards, the segmented drill model is registered to the designed CAD model. The transformation ${}^{ee}_{t}\boldsymbol{T}_{CAD}$ denotes the drill tip frame $\{t\}$ with respect to the robot end effector frame $\{ee\}$ measured in the designed CAD model. The black line demonstrates the real drilling axis. Its unit vector is $\boldsymbol{v} = [v_x, v_y, v_z]$, as shown in Fig.4. The position error $\boldsymbol{p}_e = [x, y, 0]^T$ is the intersection of the drill axis vector $\boldsymbol{v}$ with the $\boldsymbol{x}_t - \boldsymbol{y}_t$ plane of the drill tip frame in the CAD model. Then, the rotation error

of the drill system is also compensated. The rotation errors are φ and θ, which are roll and pitch rotation angles around the $\boldsymbol{x}_t$- and $\boldsymbol{y}_t$-axes, respectively. The orientation errors are computed from the following equations:

$$\varphi = \text{atan}(-v_y, v_z), \tag{1}$$

$$\theta = \text{atan}(v_x, \sqrt{v_y^2 + v_z^2}). \tag{2}$$

Then, the registration matrix $\boldsymbol{T}_v$ is generated by using the position and rotation errors:

$$\boldsymbol{T}_v = \begin{bmatrix} \boldsymbol{R}_v & \boldsymbol{p_e} \\ \boldsymbol{0}_{1\times 3} & 1 \end{bmatrix}, \tag{3}$$

where $\boldsymbol{R}_v$ is the rotation matrix generated from the Euler angles φ and θ. After calibration, the actual transformation ${}^{ee}_{t}\boldsymbol{T}$ between the drill tip frame and the robot end effector frame is calculated as ${}^{ee}_{t}\boldsymbol{T} = {}^{ee}_{t}\boldsymbol{T}_{CAD}\ \boldsymbol{T}_v$. In case of modification to the drilling system, the registration has to be repeated to ensure registration accuracy.

B. US Reconstruction and CT-to-US Registration

Before scanning, several predetermined points are manually selected on the skin surface at the level of the lumbar spine using admittance control. This hands-on operation emulates a surgeon's freehand technique without the need for an external camera. The scanning path is derived as an S-shaped motion path covering the area taught by the operator. To sufficiently cover the region of interest (ROI), a distance between the subsequent poses of around 25 to 30 mm is maintained.

The employed scanning and reconstruction algorithm is described in previous research [30]. The scanning process is carried out automatically at 4 mm/s using hybrid control while maintaining a constant force of 5 N along the probe z_{us}-axis. This force ensures optimal image quality without inducing tissue displacement. The hybrid position and force control algorithm establishes a velocity-based controller between the predefined poses and measured forces along z_{us}-axis. The mass-damper-spring relation is applied to the other axes to convert the interaction force with the environment to a reference pose for the velocity controller. The proposed algorithm establishes an integral-based controller between the pose deflection and force error along z_{us}-axis:

$$\tilde{p}_{z_{us}} = c_{us} \int f_e dt, \tag{4}$$

where $\tilde{p}_{z_{us}}$ is the pose deviation along the US probe z-axis, and c_{us} is the compliance coefficient. A high value for the compliance coefficient increases the tracking speed of the robot end effector with respect to surface fluctuations over the scanning path. The compliance coefficient is fine-tuned as 1.5 mm/sN.

Figure 5 shows the reconstruction and registration pipeline. A deep learning network, U-Net, is developed for realizing automatic image segmentation [31]. Before the experiment, 300 US images of 1080×1920 pixels are manually collected from several spine specimens. Those images are used in training and excluded from the validation. Then, the images are cropped to 800×800 pixels and manually labelled for training. Then, the images are augmented by mirroring and shifting on vertical and horizontal axes separately to increase the training dataset. The model is trained with the augmented images and applied for image segmentation.

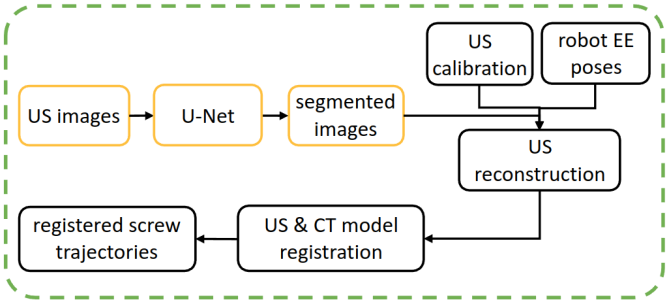

Fig. 5. Workflow of the US-based navigation system.

During the experiments, new US images are collected with the corresponding poses in the robot base frame. The raw images are cropped to 800×800 pixels. Then, the processed images are segmented by the trained network. Subsequently, threshold and Canny Edge detection are applied to extract the bone contours. The reconstruction algorithm takes the US image sequences and corresponding robot end effector poses ${}^{b}_{ee}\boldsymbol{T}$ simultaneously as input to generate 3D points. Subsequently, the pixels of segmented contour ${}^{i}\boldsymbol{p} = (\boldsymbol{w}, \boldsymbol{u})$ are converted into a point cloud ${}^{b}\boldsymbol{p} = (\boldsymbol{x}, \boldsymbol{y}, \boldsymbol{z})$ that is expressed in the robot base frame:

$${}^{b}\boldsymbol{p} = {}^{b}_{ee}\boldsymbol{T}\ {}^{ee}_{i}\boldsymbol{T}\ \boldsymbol{T}_s\ {}^{i}\boldsymbol{p}. \tag{5}$$

The next step is to find the transformation ${}^{b}_{CT}\boldsymbol{T}$ of the CT frame $\{CT\}$ to the robot base frame $\{b\}$, with associated screw trajectories ${}^{CT}\boldsymbol{s}$. This is done by registering the US reconstructed point cloud in the robot base frame with the preoperative CT model in the CT frame $\{CT\}$. The registration is performed in two steps: (i) a pre-registration based on 4 landmarks and (ii) a refining registration based on a two-step iterative closest point (ICP) algorithm [32]. In more detail, first, the bone contour is segmented in the preoperative CT image and converted to a surface point cloud. Then, using the landmarks picked by the operator, a point-to-point pre-registration is applied, pre-aligning the CT point cloud with the 3D US point cloud as an initial guess for the second step. Finally, the ICP registration algorithm is applied to refine the registration automatically.

Using the registration transformation matrix, the preoperative CT image and associated screw trajectories ${}^{CT}\boldsymbol{s}$ are transformed into the robot base frame as ${}^{b}\boldsymbol{s}$ such that they align with the patient as follows:

$${}^{b}\boldsymbol{s} = {}^{b}_{CT}\boldsymbol{T}\ {}^{CT}\boldsymbol{s}. \tag{6}$$

The development and validation of the reconstruction and registration accuracy have been performed in previous work [33].

C. Robotic Drilling

Knowing the screw trajectory ${}^{b}\boldsymbol{s} = [\boldsymbol{p}_{ep}, \boldsymbol{p}_{sp}] = [x_{ep}, y_{ep}, z_{ep}, x_{sp}, y_{sp}, z_{sp}]$ with respect to the robot base

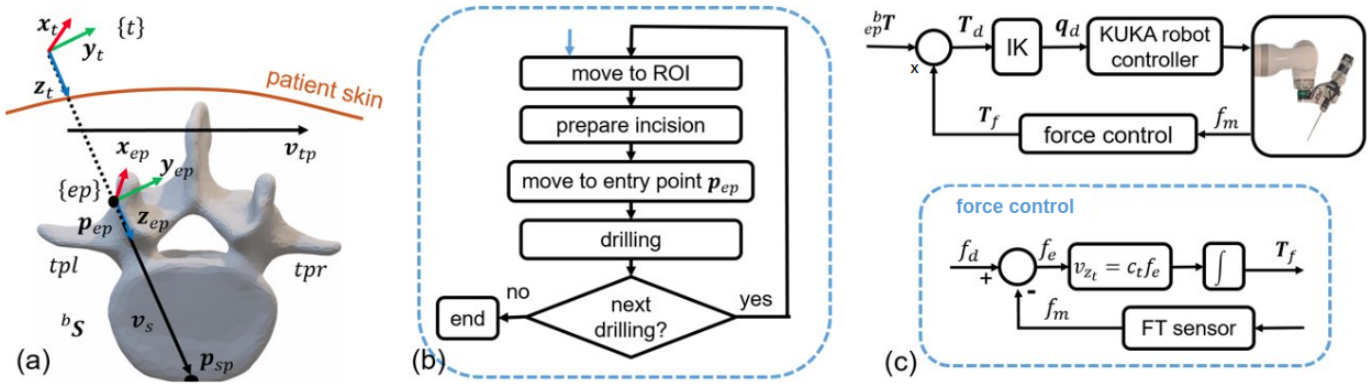

Fig. 6. (a) Definition of the local entry point frame $\{ep\}$ with a predefined screw trajectory ${}^{b}\boldsymbol{s}$ for a vertebra. (b) Block diagram of the automatic drilling after the screw trajectory registered to the robot base frame by using US navigation. (c) The proposed position/force control block diagram for the drilling procedure.

frame, the drill will automatically conduct on the vertebrae. The entry point and stop point for each vertebra are used to generate the screw vector as $\boldsymbol{v}_s = \boldsymbol{p}_{sp} - \boldsymbol{p}_{ep}$. For each vertebra, a supplementary vector $\boldsymbol{v}_{tp} = \boldsymbol{p}_{tpr} - \boldsymbol{p}_{tpl}$ from the left transverse processes (tpl) to the right transverse processes (tpr) is also defined, as shown in Fig.6 (a). The $\boldsymbol{p}_{ep}$ is the origin of the entry point frame. By using $\boldsymbol{v}_{tp}$ and $\boldsymbol{v}_s$, the local entry point frame $\{ep\}$ can be established as follows:

$$\boldsymbol{z}_{ep} = \frac{\boldsymbol{v}_s}{|\boldsymbol{v}_s|}, \tag{7}$$

$$\boldsymbol{x}_{ep} = \frac{\boldsymbol{v}_{tp} \times \boldsymbol{z}_{ep}}{|\boldsymbol{v}_{tp} \times \boldsymbol{z}_{ep}|}, \tag{8}$$

$$\boldsymbol{y}_{ep} = \boldsymbol{z}_{ep} \times \boldsymbol{x}_{ep}, \tag{9}$$

$$\boldsymbol{R}_{ep} = [\boldsymbol{x}_{ep}\, \boldsymbol{y}_{ep}\, \boldsymbol{z}_{ep}], \tag{10}$$

where $\boldsymbol{x}_{ep}$, $\boldsymbol{y}_{ep}$, $\boldsymbol{z}_{ep}$, and $\boldsymbol{R}_{ep}$ are the unit normal vectors and the corresponding rotation matrix, respectively. Then, the transformation ${}^{b}_{ep}\boldsymbol{T}$ denotes the entry point frame $\{ep\}$ with respect to the robot base frame $\{b\}$ as follows:

$${}^{b}_{ep}\boldsymbol{T} = \begin{bmatrix} \boldsymbol{R}_{ep} & \boldsymbol{p}_{ep} \\ \boldsymbol{0}_{1\times 3} & 1 \end{bmatrix}. \tag{11}$$

After defining the entry point frame $\{ep\}$, the drill automatically moves to 5 cm above the ROI with position control. The orientation of the drill bit follows the predefined trajectory. Then, the surgeon makes an incision and places the dilator through the incision. The drill bit approaches the entry point along the z_{ep}-axis with a constant 1 mm/s speed while keeping the orientation. The workflow of the automatic drilling is illustrated in Fig.6 (b).

After reaching the desired entry point, the operator prepares the entry point with a custom-designed surgical awl. Subsequently, the robot drills the bone along the planned trajectory. The implemented hybrid position and force control strategy keeps the drill tip aligned and exerts a constant force along the drilling direction. The penetration speed is 1 mm/s along z_t-axis, while the desired drilling force is regulated at approximately 20 N. The control block diagram is shown in Fig.6 (c). The drilling axis is force-controlled to have precise guidance over the drill bit, and for the other 5 degrees of freedom (DoFs), position control is used. The interaction force f_m measured in the sensor frame is transformed to the drill tip frame $\{t\}$. To have a safe and constant force drilling, an admittance law converts force error f_e to a corresponding velocity in the drill tip z_t direction v_{z_t}:

$$v_{z_t} = c_t\, f_e = c_t\, (f_d - f_m), \tag{12}$$

where v_{z_t}, c_t, and f_d are the velocity of the displacement along drill tip z_t-axis, the compliance coefficient, and the desired force, respectively. By integration of the v_{z_t}, the position displacement becomes $\boldsymbol{p}_f = [0, 0, \int v_{z_t}]$ in the drill tip frame $\{t\}$. Then, the transformation matrix $\boldsymbol{T}_f$ computed from the force control becomes as follows:

$$\boldsymbol{T}_f = \begin{bmatrix} \boldsymbol{I} & \boldsymbol{p}_f \\ \boldsymbol{0}_{1\times 3} & 1 \end{bmatrix}. \tag{13}$$

During drilling, the desired pose of the drill tip $\boldsymbol{T}_d$ is the product of the pre-planned trajectory ${}^{b}_{ep}\boldsymbol{T}$ and $\boldsymbol{T}_f$. Then, the applied pose is fed to the inverse kinematics of the robot to find the corresponding desired joint angles $\boldsymbol{q}_d$. Based on the desired joint angles, the required torques for each joint are calculated internally by the robot controller.

IV. Experiments and Evaluation

This section presents the experimental setup employed in this study. Subsequently, the ex-vivo spines are described. The experiments were conducted on both ex-vivo lamb and human spines. Then, detailed evaluation criteria based on both geometric and clinical aspects are introduced.

A. Experimental Setup

Figure 7 shows the experimental setup consisting of a US imaging system (GE Loqiq 7, GE Healthcare, USA), a custom-designed drill and a lightweight robotic arm (KUKA Robot MED7, Augsburg, Germany). The US system uses a 7.5 MHz linear probe. A frame grabber (Epiphan Systems Inc. Palo Alto, Canada) is employed to capture US images via a USB port at 50 Hz. A custom-designed US probe holder and motorized drill are designed for the robot end effector and separately assembled by a fast tool changer (G-SHW063-2UE, GRIP GmbH, Germany). A custom-designed drill controller controls the speed and provides power for the drill bit. For each, a 6 DoFs force torque sensor (Nano25, ATI Industrial Automation

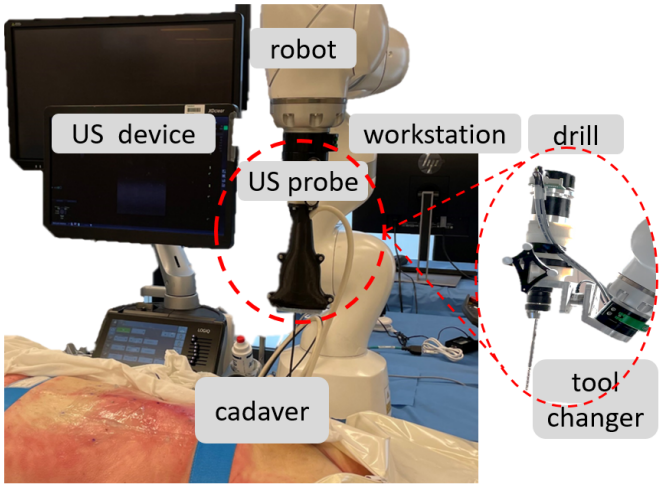

Fig. 7. The experimental setup of the proposed system, including the robot-assisted US system and drilling system. After US scanning, the US probe is disassembled and the drilling system is connected to the robot end effector by using the tool changer.

Inc.) is assembled at the US probe and the drilling system. A PC workstation (Intel i7, CPU @2.6 GHz, 64G RAM) is used for data acquisition and processing. The PC runs Ubuntu 20.04 and Robot Operating System (ROS). For real-time robot control, Open Robot Control Software (Orocos, version 2.9.0) is employed and operates at 200 Hz. For image processing and visualization, custom-designed software is developed and integrated with OpenCV (Intel Corporation, USA) and Visualization Toolkit (https://www.vtk.org). The GUI for human-computer interaction is developed with the open-source toolkit QT (https://www.qt.io). An NVIDIA A4500 and NVIDIA Compute Unified Device Architecture (CUDA) are used to accelerate the processing and computation. The robot and FT sensor communicate with the workstation via Ethernet.

B. Ex-vivo Lamb Spines

Prior to the experiments, the operator segmented the CT images and reconstructed the spine as a 3D model by using ITK-snap [34]. The drilling trajectories were identified on the 3D model as shown in Fig.6 (a). The predetermined trajectory was defined by the entry point on the surface of the pedicle and the stop point on the vertebrae body surface. The entry point and stop point along the trajectory were marked on the CT model.

The experiments were conducted on three ex-vivo lamb spines. Each lamb spine contained six vertebrae, as shown in Fig.8. The skin and fat were removed to ensure a good US image quality. The lamb spine was fixed by using screws from the side to avoid motion during US scanning. For each lamb spine, 8 trajectories were predefined on four vertebrae by the operator, resulting in 24 drilling trajectories for quantitative assessment.

C. Ex-vivo Human Spines

The experiment was also conducted on three fresh-frozen human spines. Ethical approval was granted by the Belgian National Council for Bioethics for this study. The main inclusion

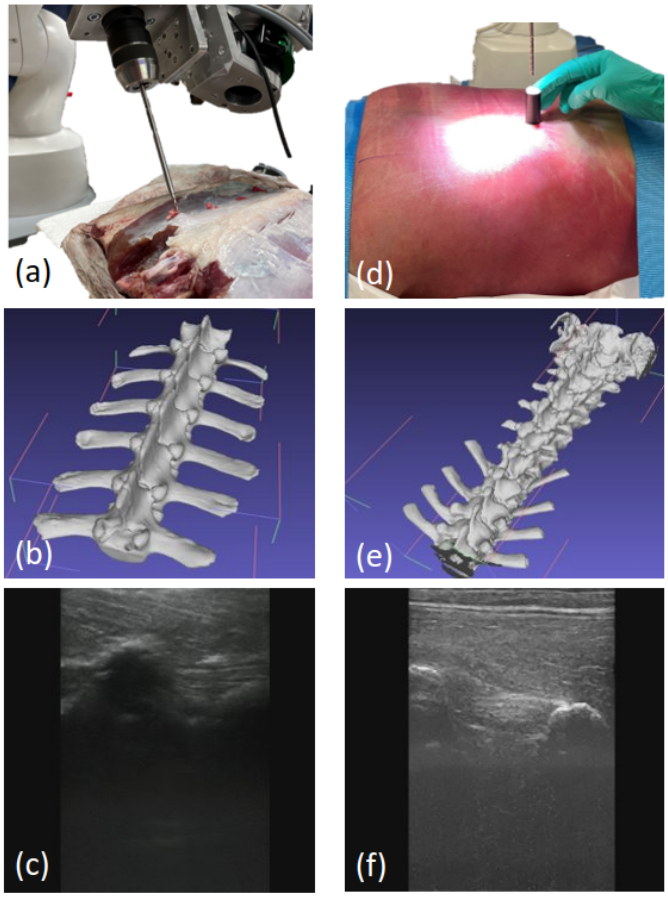

Fig. 8. (a) An ex-vivo lamb spine attached to the operating table under the robotic drill. The skin and fat layers are removed to offer a better US image quality. (b) The preoperative CT model of the lamb spine. (c) An example of the US images from a lamb spine. (d) The ex-vivo human spine with intact skin is fixed by two straps. (e) The preoperative CT model of the human spine. (f) An example of the US images from a human cadaver.

criteria were: no previous interventions on the spine; no overweight (body mass index $\leq$ 30.0 kg/m^2); no scoliosis. The cadaver was positioned prone and fixed on the surgical bed to avoid motion using two straps. The drill trajectory was determined based on the patient-specific planning that was described in detail in [35]. In total, 16 trajectories were defined through the pedicles from T10 to L5 on the preoperative CT scan. For all the surgical plans, trajectories were selected to prevent lateral and medial breaches. The entry and stop points along the drill trajectory were manually annotated in the postoperative CT model for evaluation.

However, only one of the human cadavers was reported in this paper. One of the human cadavers was excluded because it had scoliosis, which was considered too challenging for a first proof of principle. The second human cadaver was excluded due to the bad bone quality; the preoperative and postoperative CT were not validated.

D. Evaluation Criteria

For evaluation, the preoperative and postoperative CT scans were conducted separately before scanning and after drilling. The cadavers kept the same posture during the CT scan as

during the operation. For comparison, the preoperative and postoperative CT models were registered in the 3D space.

1) Positioning Error: The errors of the entry point e_{ep} and stop point e_{sp} are calculated as the shortest distance between the measured entry point and the line connecting the planned entry and destination points, as described in [33]. When evaluating the system positioning accuracy, the rotation around z_{ep}-axis is not considered because the screw would move along the trajectory [36]. The orientation around the z_{ep}-axis of the screw trajectory is also not measured since the screw is axisymmetric and this roll angle is not clinically relevant. The orientation error e_θ, thus mostly error in inclination, is computed as the angle between the vector of planned trajectory $\mathbf{v}_{s,pre}$ in the preoperative CT model and drilled vector $\mathbf{v}_{s,post}$ in the postoperative CT model according to [37] as follows:

$$\boldsymbol{v}_{s,pre} = \boldsymbol{p}_{sp,pre} - \boldsymbol{p}_{ep,pre}, \tag{14}$$

$$\boldsymbol{v}_{s,post} = \boldsymbol{p}_{sp,post} - \boldsymbol{p}_{ep,post}, \tag{15}$$

$$e_\theta = \frac{\boldsymbol{v}_{s,pre} \cdot \boldsymbol{v}_{s,post}}{||\boldsymbol{v}_{s,pre}|| \ ||\boldsymbol{v}_{s,post}||}. \tag{16}$$

2) Gertzbein-Robbins Grade: The Gertzbein-Robbins (GR) grade [18] is evaluated by extrapolating the drill bit diameters to common pedicle screw diameters. In surgery, the diameter of the pedicle screw typically varies from 4 to 7 mm [38]. The position of each pedicle screw is evaluated with the GR grading system on postoperative CT images obtained by using 3D Slicer [39]. Grade A screws are within the pedicle; grade B screws breach the cortex of the pedicle by ≤ 2 mm; grade C screws breach the pedicle wall by 2 to 4 mm; grade D screws breach the pedicle wall by 4 to 6 mm; grade E screws breach pedicle wall by ≥ 6 mm. Grade A or B screws are considered as clinically acceptable [40]. When the maximum cortical breach is $\leq$2 mm, the corresponding grade is defined as 1; otherwise, it is 0. Clinical accuracy is calculated by analyzing the grades of all the drilled screw trajectories. In the present study, this evaluation is used to assess the experiments on the human cadaver spines with a screw diameter of 6 mm. The criterion is not suitable for lamb spines, as the pedicle area in the lamb is much smaller than in humans.

V. Results

A. Positioning Error on Ex-vivo Lamb Spines

In total, 24 drillings were conducted on three ex-vivo lamb spines. The experimental results for position and orientation errors are described in Table I.

TABLE I
Results of the position and orientation error of 24 drilled trajectories on three ex-vivo lamb spines.

Lamb specimens	Entry point error e_{ep} [mm]	Stop point error e_{sp} [mm]	Orientation error e_θ [°]
1	2.10±0.93	2.91±1.14	3.06±1.11
2	1.51±0.82	2.64±1.87	2.04±1.80
3	3.55±1.56	4.20±2.17	3.36±2.37
Mean	2.39±1.41	3.25±1.84	2.82±1.85

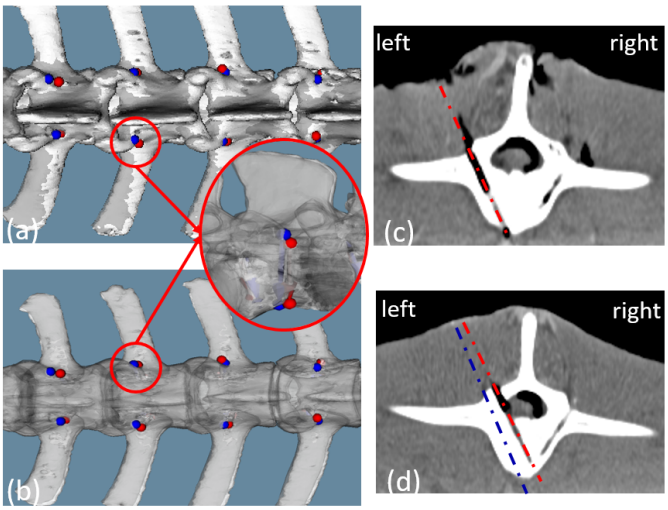

Fig. 9. The demonstration of registered postoperative CT model (gray) and drilled screw trajectories (red) overlaid with the preoperative CT model (white) and surgical plans (blue) from (a) top view and (b) bottom view. Examples of the postoperative CT scan on the ex-vivo lamb spine with (c) a non-breach trajectory and (d) a breach trajectory.

The mean position errors are 2.39 ± 1.41 mm and 3.25 ± 1.84 mm for the entry point and stop point, respectively. The errors at the stop point are larger than those at the entry point, as the orientation errors propagate to position errors. The maximum entry point error is 3.55 ± 1.56 mm on specimen 3, while the maximum orientation error is $3.36 \pm 2.37°$.

Figure 9 demonstrates the results of lamb 2. The postoperative CT model in gray is registered with the preoperative CT model in white. There are two examples of the drill trajectory in postoperative CT images with non-breach Fig.9 (c) and medial breach Fig.9 (d).

B. Positioning Error on Ex-vivo Human Spines

Table II demonstrates the accuracy of the proposed system on the ex-vivo human spine. The entry point error yields 2.26 ± 1.95 mm on the left side and 3.90 ± 2.79 mm on the right side. The mean position error is 3.08 ± 2.43 mm at the entry point and 4.05 ± 2.62 mm at the stop point across 16 drilling trajectories. The mean orientation error is $2.05 \pm 0.85°$. The minimum

TABLE II
Results of the position and orientation error of drilling trajectory on ex-vivo human spine.

Vertebrae level	e_{ep} [mm]		e_{sp} [mm]		e_θ [°]	
	Left	Right	Left	Right	Left	Right
T10	1.03	7.20	1.83	7.23	1.22	1.84
T11	1.10	6.43	3.03	6.19	2.44	2.26
T12	1.23	7.28	1.78	5.24	2.51	2.92
L1	5.37	2.21	5.88	2.38	0.70	0.87
L2	0.58	3.15	1.20	1.86	0.73	1.77
L3	2.60	3.05	4.96	2.65	2.42	2.28
L4	5.17	0.35	7.68	2.87	2.89	2.74
L5	1.04	1.56	9.33	0.70	3.55	1.63
Mean	2.26	3.90	4.46	3.64	2.06	2.04
STD	1.95	2.70	3.00	2.30	1.05	0.66

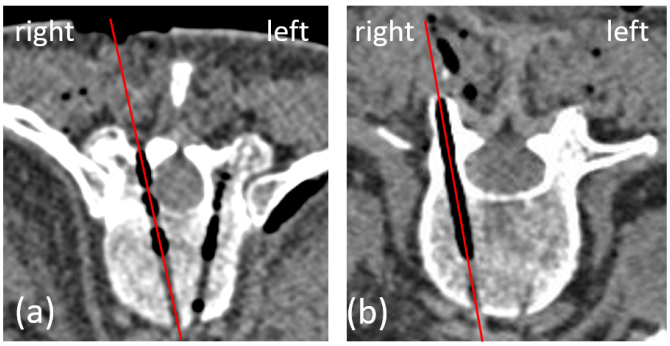

Fig. 10. Examples of drilled trajectories on the postoperative CT scan with (a) grade C at T10 and (b) grade A at L3 of the ex-vivo human spine. The red lines indicate the drilled trajectories.

position error is 0.58 mm at the entry point and 1.20 mm at the stop point for the L2 left side.

Figure 10 demonstrates the postoperative CT of the human spine at T10 and L3. The drilling procedures stop by going through the cortical layer of the vertebral body. The drill trajectory is located in the middle of the pedicle area without medial breach for L3.

Figure 11 shows the measured force along the drill tip z_t-axis. The force decreases between 6 to 15 seconds when drilling through the vertebral body with a medial breach, as shown in Fig.11 (a). The force also reduces to less than 6 N when the drill tip encounters the cancellous layer. Conversely, the force increases significantly as the drill bit approaches the cortical layer. The demonstrated force corresponds to the medial breach drilling in Fig.10(a).

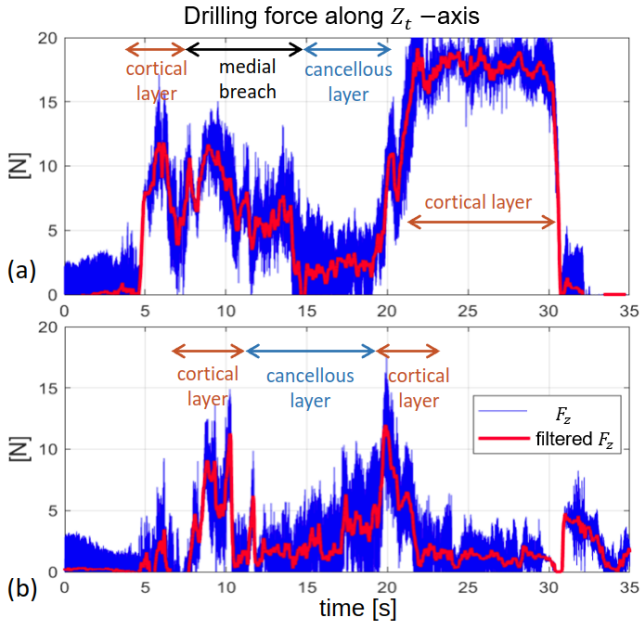

Fig. 11. Examples of the force along the trajectory during drilling with (a) a medial breach and (b) no breach on the ex-vivo human spine. The blue line represents the raw measurement, while the red line is the filtered data.

C. Gertzbein-Robbins Grade on Ex-vivo Human Spines

Table III shows the GR grade following the measured drilled screw trajectory on ex-vivo human spines. With a screw diameter of 6 mm, the results report 10 grade A trajectories and 4 grade B trajectories. In total, an 87.5% success rate while all breaches remain within 2 mm. However, there are two drills that are categorized as grade C, namely at T10 right and L5 left. The maximum orientation error is 3.55° on L5 left, while it results in a maximum position error 9.33 mm at the stop point.

TABLE III
GR GRADE OF DRILLED TRAJECTORIES ON THE HUMAN CADAVER SPINE

Vertebrae level	GR grade	
	Left	Right
T10	A	C
T11	A	B
T12	A	B
L1	B	A
L2	A	A
L3	A	A
L4	B	A
L5	C	A

VI. Discussion

This study represents the first investigation of an US-based robotic system for MIPSP by combining navigation and drilling procedures. This US-based approach could potentially result in a 100% intraoperative radiation dose reduction for both patient and surgeon.

A. Validation on Ex-vivo Lamb Spines

A previous research demonstrated that the proposed US-based navigation system achieved 2.80 ± 1.14 mm position error and $1.38 \pm 0.61°$ orientation error [33]. The proposed system could guarantee a similar navigation performance as other research [20], [41]. Expanding upon this work to incorporate the drilling procedure, the system attained a mean position error of 2.39 ± 1.41 mm mean position error at the entry point and $2.82 \pm 1.85°$ rotation error on lamb spines as shown in Table I.

While the US offers several advantages, including affordability, safety, and real-time imaging, its effectiveness can be hindered by lower spatial resolution compared to CT and fluoroscopy. One can notice that the accuracy of lamb specimen 3 exhibited inferior accuracy compared to the other two specimens. This is probably due to the image contrast being lower on lamb specimen 3, while the bone contours are blurred in the raw images. while there are still some challenges to tackle before adopting the approach in clinical practice. With a systematic approach, appropriate training, and the implementation of the latest US technologies, these challenges could be significantly mitigated. Combined with such patient selection, the proposed approach would be able to treat a portion of the patients with showing high clinical value.

Additionally, there is no guarantee that the US images will capture all bone features present in the preoperative CT model. It is a challenge to optimize the registration by using limited overlap. Therefore, the CT to US registration could

TABLE IV
COMPARISON OF SCREW PLACEMENT ACCURACY

Study	Surgical approach	Navigation	Robot	Model	Number of screws	Technical accuracy [mm]		Clinical accuracy [%]
						Entry point	Stop point	
Smith *et al.* [26]	Open	Optical system	KUKA LBR	Phantom	10	0.49±0.17	1.49±0.46	-
Jiang *et al.* [44]	Open	Optical system	Excelsius GPS	Patient	8	2.11±1.42	3.18±1.29	100
Gao *et al.* [45]	MIS	Fluoroscopy	UR 10	Cadaver	10	5.10±2.40	-	-
Bakhtiarinejad *et al.* [37]	MIS	Fluoroscopy	UR 10	Cadaver	8	3.64±0.67	3.78±0.68	-
Current study	MIS	Ultrasound	KUKA MED7	Cadaver	16	3.08±2.43	4.05±2.62	87.5

still be improved. There are several researchers who propose automatic US to CT registration. Brößner *et al.* provided a comprehensive comparison of deep learning-based registration with validation on 3D printed carpal phantom for percutaneous scaphoid fixation [42]. With that proposed system, the screw placement achieves 1.0 ± 0.6 and 0.7 ± 0.3 mm at the distal and proximal pole, respectively.

However, one should also remark that it is not easy to distinguish between navigation system errors and drilling procedure errors, as only the final accuracy is assessed in this work. Several factors also affect the screw placement accuracy, such as skiving at a bony surface and incorrect drill force [43]. During lamb experiments, it was noticed that the drill bit deformed slightly owing to skiving. It is important to determine a well-chosen bone entry point and prepare it by removing the surrounding soft tissue with a surgical awl. This action also could have reduced the drilling accuracy and increased positioning error. Additionally, the drilling system exhibited wobbling movement around z_t-axis, generating around 1 mm position error.

B. Validation on Ex-vivo Human Spine

For the ex-vivo human spine, the position error and deviation slightly increase to 3.08 ± 2.43 mm and 4.05 ± 2.62 mm at the entry and stop point. A potential reason for that is the soft tissue in the human body is more complex than that of lamb. It is found difficult to segment all the anatomic features (i.e., spinous process) from human cadaver spines.

Figure 10 depicts two drilling trajectories on a human cadaver, showing a grade C breach at T10 and a grade A trajectory at L3. It is observed that the first drill on L5 left and the last drill on T10 right result in breaches larger than 2 mm. Compared to the lamb spine, the human back presents a larger region of interest measuring approximately 400 mm $\times$ 200 mm. During the experiment, the locations of T10 and L5 are close to the boundary of the robot workspace. The calibration accuracy determined in the center area of the robot workspace may have been affected by the difficulty in reaching the desired position around the boundary while maintaining good joint accuracy and calibration accuracy. Additionally, a grade B trajectory occurred on L1 left due to the drill bit skived over the pedicle area.

When the drill moves through the pedicle, the force indicates the drilling state on different bone layers. Lower forces are encountered when drilling through the cancellous layer, which has a honeycombed structure and experiences minimal mechanical stress. In contrast, the drilling force peaks at the exact moment of the breach. Utilizing force-based sensory feedback could potentially provide a breach algorithm to detect or stop the drilling in case of a hazard for the patient [9].

From a technical point of view, Table IV puts in perspective the results of this study with those of prior research. Smith *et al.* reported the entry point accuracy was 0.49 ± 0.17 mm and the destination point accuracy was 1.49 ± 0.46 mm by using an optical tracking system [26]. However, it required the operator to manually register the phantom, which could have influenced the final accuracy. Gao *et al.* presented a robotic spine needle injection system using fluoroscopic image-based navigation, achieving a mean translation error of 5.1 mm and an orientation error of 3.6 degrees [45]. Similarly, Bakhtiarinejad *et al.* implemented a robotic system with a multiview C-arm and achieved distance errors of 3.28 mm and 2.64 mm for entry and target points on human cadavers [37]. Our system demonstrates comparable performance, with a mean position accuracy of 2.57 mm and orientation accuracy of 1.71 degrees in 14 successful trajectories (i.e., grade A and B trajectories). When including grade C trajectories, position errors increase to 3.08 ± 2.43 mm and 4.05 ± 2.62 mm at the entry and stop points, respectively. While such performance is promising and compared well with state-of-the-art studies on MIS approaches, the accuracy of our proposed system could still be improved to meet the accuracy of open surgery approaches.

From a clinical point of view, this study provides a feasibility assessment in a pre-clinical setting with detailed experimental specifications. The proposed system achieves an 87.5% success rate using GR grade. For comparison, existing studies have reported clinical assessments using commercial robot-assisted systems. Jiang *et al.* reported a 100% clinically acceptable rate on two patients, with seven screws graded A and one graded B [44]. MIPSP offers an alternative to open surgery by achieving promising results while minimizing patient harm. By using US navigation, the developed system significantly reduces intraoperative radiation exposure for both patients and surgeons. However, the proposed system remains a prototype, requiring further advancements to achieve the level of precision met with the open surgery systems.

C. Current Challenges and Future Work

While the feasibility of the proposed system has been validated, several important components must be investigated prior to clinical use.

Firstly, the execution time of the intraoperative navigation and drilling is not discussed. Currently, the proposed systems may suffer from the lag between user input and system response, impacting surgical workflow. The procedure may take longer

than the conventional approach because of safety features. Future research should focus on minimizing response times to ensure smooth and efficient surgical procedures.

Secondly, in-vivo investigation and validation must be taken into account. The proposed system does not yet deal with physiological motion and breach prediction. It is important to develop motion compensation strategies for both US navigation and drilling to improve the system performance. Meanwhile, incorporating a breach prediction algorithm would enable the system to manage hazardous situations and prevent patient harm.

Finally, future work will need to focus on developing infrastructure solutions, including ergonomic equipment and training programs, to address the transition from the established workflow with fluoroscopy to a US-based approach. Expanding the system from a single robot to two robots where one robot does US scanning and another one is responsible for drilling could shorten the procedure and potentially allow improved motion compensation and help compensate for the error simultaneously.

VII. Conclusion

This paper proposes a US-based robotic system for MIPSP. Traditional PSP procedures heavily rely on fluoroscopy-guided instrumentation, exposing both the patient and surgeon to radiation. This work provides preliminary results showing the feasibility of US-guided robot-assisted MIPSP. The proposed robotic system holds the potential to revolutionize spinal surgery, offering several compelling advantages. Its non-radiative and fiducial-free design expands its applicability to a wider range of patients. Further work is needed to establish which factors contribute to what extent to the remaining error and how to lower their impact in real clinical practice.

Acknowledgments

The authors would like to express their gratitude to Ann Van Ermen and Kristof Reyniers at the UZ Leuven Anatomy and Surgical Technologies Skills Centre for their assistance in organizing the study and preparing the anatomy. Additionally, the authors would like to extend their appreciation to Walter Coudyzer for his contribution to taking CT scans.

References

[1] K. T. Huntsman, L. A. Ahrendtsen, J. R. Riggleman, and C. G. Ledonio, "Robotic-assisted navigated minimally invasive pedicle screw placement in the first 100 cases at a single institution," *Journal of Robotic Surgery*, vol. 14, no. 1, pp. 199–203, 2020.

[2] M. Shoham, M. Burman, E. Zehavi, L. Joskowicz, E. Batkilin, and Y. Kunicher, "Bone-mounted miniature robot for surgical procedures: Concept and clinical applications," *IEEE Transactions on Robotics and Automation*, vol. 19, no. 5, pp. 893–901, 2003.

[3] A. A. Aoude, M. Fortin, R. Figueiredo, P. Jarzem, J. Ouellet, and M. H. Weber, "Methods to determine pedicle screw placement accuracy in spine surgery: a systematic review," *European Spine Journal*, vol. 24, no. 5, pp. 990–1004, 2015.

[4] N. Beisemann, J. Gierse, E. Mandelka, F. Hassel, P. A. Grützner, J. Franke, and S. Y. Vetter, "Comparison of three imaging and navigation systems regarding accuracy of pedicle screw placement in a sawbone model," *Scientific Reports*, vol. 12, no. 1, p. 12344, 2022.

[5] I. B. Lopez, A. Benzakour, A. Mavrogenis, T. Benzakour, A. Ahmad, and J.-M. Lemée, "Robotics in spine surgery: systematic review of literature," *International Orthopaedics*, vol. 47, no. 2, pp. 447–456, 2023.

[6] Z. Jiang, S. E. Salcudean, and N. Navab, "Robotic ultrasound imaging: State-of-the-art and future perspectives," *Medical Image Analysis*, p. 102878, 2023.

[7] Z. Jiang, Y. Gao, L. Xie, and N. Navab, "Towards autonomous atlas-based ultrasound acquisitions in presence of articulated motion," *IEEE Robotics and Automation Letters*, vol. 7, no. 3, pp. 7423–7430, 2022.

[8] G. Burström, M. Balicki, A. Patriciu, S. Kyne, A. Popovic, R. Holthuizen, R. Homan, H. Skulason, O. Persson, E. Edström *et al.*, "Feasibility and accuracy of a robotic guidance system for navigated spine surgery in a hybrid operating room: a cadaver study," *Scientific reports*, vol. 10, no. 1, p. 7522, 2020.

[9] Z. Jiang, L. Lei, Y. Sun, X. Qi, Y. Hu, B. Li, N. Navab, and J. Zhang, "Model-based compensation of moving tissue for state recognition in robotic-assisted pedicle drilling," *IEEE Transactions on Medical Robotics and Bionics*, vol. 2, no. 3, pp. 463–473, 2020.

[10] C. J. Kleck, C. Johnson, M. Akiyama, E. L. Burger, C. J. Cain, and V. V. Patel, "One-step minimally invasive pedicle screw instrumentation using o-arm and stealth navigation," *Clinical Spine Surgery*, vol. 31, no. 5, pp. 197–202, 2018.

[11] B. Felix, S. B. Kalatar, B. Moatz, C. Hofstetter, M. Karsy, R. Parr, and W. Gibby, "Augmented reality spine surgery navigation: increasing pedicle screw insertion accuracy for both open and minimally invasive spine surgeries," *Spine*, vol. 47, no. 12, pp. 865–872, 2022.

[12] C. W. Kim, Y.-P. Lee, W. Taylor, A. Oygar, and W. K. Kim, "Use of navigation-assisted fluoroscopy to decrease radiation exposure during minimally invasive spine surgery," *The Spine Journal*, vol. 8, no. 4, pp. 584–590, 2008.

[13] I. D. Gelalis, N. K. Paschos, E. E. Pakos, A. N. Politis, C. M. Arnaoutoglou, A. C. Karageorgos, A. Ploumis, and T. A. Xenakis, "Accuracy of pedicle screw placement: a systematic review of prospective in vivo studies comparing free hand, fluoroscopy guidance and navigation techniques," *European spine journal*, vol. 21, no. 2, pp. 247–255, 2012.

[14] J. Du, L. Gao, D. Huang, L. Shan, W. Wang, Y. Fan, D. Hao, and L. Yan, "Radiological and clinical differences between robotic-assisted pedicle screw fixation with and without real-time optical tracking," *European Spine Journal*, vol. 30, no. 1, pp. 142–150, 2021.

[15] Lefranc, M., Peltier, J., "Accuracy of thoracolumbar transpedicular and vertebral body percutaneous screw placement: coupling the rosa® spine robot with intraoperative flat-panel ct guidance—a cadaver study," *Journal of Robotic Surgery*, vol. 9, p. 331–338, 2015.

[16] Godzik, J., Walker, C. T., Hartman, C., de Andrada, B., Morgan, C. D., Mastorakos, G., Chang, S., Turner, J., Porter, R. W., Snyder, L. and Uribe, J., "A quantitative assessment of the accuracy and reliability of robotically guided percutaneous pedicle screw placement: Technique and application accuracy." *Operative neurosurgery (Hagerstown, Md.)*, vol. 17, p. 389–395, 2019.

[17] N. Lonjon, E. Chan-Seng, V. Costalat, B. Bonnafoux, M. Vassal, and J. Boetto, "Robot-assisted spine surgery: feasibility study through a prospective case-matched analysis," *European Spine Journal*, vol. 25, pp. 947–955, 2016.

[18] S. Robbins and S. Gertzbein, "Accuracy of pedicle screw placement in vivo," *Journal of Orthopaedic Trauma*, vol. 3, no. 2, p. 161, 1989.

[19] C. Barbe, J. Troccaz, B. Mazier, and S. Lavallee, "Using 2.5d echography in computer assisted spine surgery," in *Proceedings of the 15th Annual International Conference of the IEEE Engineering in Medicine and Biology Societ*, 1993, pp. 160–161.

[20] D. Ottacher, A. Chan, E. Parent, and E. Lou, "Positional and orientational accuracy of 3-d ultrasound navigation system on vertebral phantom study," *IEEE Trans Instrum Meas*, vol. 69, no. 9, pp. 6412–6419, 2020.

[21] J. Zhang, Y. Wang, T. Liu, K. Yang, and H. Jin, "A flexible ultrasound scanning system for minimally invasive spinal surgery navigation," *IEEE Transactions on Medical Robotics and Bionics*, vol. 3, no. 2, pp. 426–435, 2021.

[22] L.-P. Zhou, R.-J. Zhang, W.-K. Zhang, L. Kang, K.-X. Li, H.-Q. Zhang, C.-Y. Jia, Y.-S. Zhang, and C.-L. Shen, "Clinical application of spinal robot in cervical spine surgery: safety and accuracy of posterior pedicle screw placement in comparison with conventional freehand methods," *Neurosurgical Review*, vol. 46, no. 1, p. 118, 2023.

[23] H.-M. Li, R.-J. Zhang, and C.-L. Shen, "Accuracy of pedicle screw placement and clinical outcomes of robot-assisted technique versus conventional freehand technique in spine surgery from nine randomized controlled trials: a meta-analysis," *Spine*, vol. 45, no. 2, pp. E111–E119, 2020.

[24] V. Ong, A. R. Swan, J. P. Sheppard, E. Ng, B. Faung, L. D. Diaz-Aguilar, and M. H. Pham, "A comparison of spinal robotic systems and pedicle screw accuracy rates: Review of literature and meta-analysis," *Asian Journal of Neurosurgery*, vol. 17, no. 04, pp. 547–556, 2022.

[25] T. Ortmaier, H. Weiss, U. Hagn, M. Grebenstein, M. Nickl, A. Albu-Schaffer, C. Ott, S. Jorg, R. Konietschke, L. Le-Tien, and G. Hirzinger, "A hands-on-robot for accurate placement of pedicle screws," in *Proceedings 2006 IEEE International Conference on Robotics and Automation, 2006. ICRA 2006.*, 2006, pp. 4179–4186.

[26] A. D. Smith, J. Chapin, P. V. Birinyi, P. V. Bhagvath, and A. F. Hall, "Automated polyaxial screw placement using a commercial-robot-based, image-guided spine surgery system," *IEEE Transactions on Medical Robotics and Bionics*, vol. 3, no. 1, pp. 74–84, 2021.

[27] W. Tian, X. Han, B. Liu, Y. Liu, Y. Hu, X. Han, Y. Xu, M. Fan, and H. Jin, "A robot-assisted surgical system using a force-image control method for pedicle screw insertion," *PloS one*, vol. 9, no. 1, p. e86346, 2014.

[28] S. Vafadar, E. Saghbiny, A. Harlé, and G. Morel, "Using a force-controlled robot for probing-based registration and automated bone drilling in pedicle screw placement procedures," in *2023 International Symposium on Medical Robotics (ISMR)*. IEEE, 2023, pp. 1–7.

[29] R. Li *et al.*, "Comparative quantitative analysis of robotic ultrasound image calibration methods," in *2021 20th International Conference on Advanced Robotics (ICAR)*. IEEE, 2021, pp. 511–516.

[30] R. Li, A. Davoodi, Y. Cai, K. Niu, G. Borghesan, N. Cavalcanti, A. Massalimova, F. Carrillo, C. J. Laux, M. Farshad *et al.*, "Robot-assisted ultrasound reconstruction for spine surgery: from bench-top to pre-clinical study," *International journal of computer assisted radiology and surgery*, pp. 1–11, 2023.

[31] O. Ronneberger, P. Fischer, and T. Brox, "U-net: Convolutional networks for biomedical image segmentation," *Lecture Notes in Computer Science.*, vol. 9351, p. 234–241, 2015.

[32] P. J. Besl and N. D. McKay, "A method for registration of 3-d shapes," *IEEE Transactions on Pattern Analysis and Machine Intelligence*, vol. 14, no. 2, pp. 239–256, 1992.

[33] R. Li, A. Davoodi, Y. Cai, G. Borghesan, N. Cavalcanti, C. J. Laux, M. Farshad, F. Carrillo, P. Fürnstahl, and E. Vander Poorten, "Development and evaluation of robot-assisted ultrasound navigation system for pedicle screw placement: An ex-vivo animal validation," *The International Journal of Medical Robotics and Computer Assisted Surgery*, p. e2590, 2023.

[34] P. A. Yushkevich, Y. Gao, and G. Gerig, "Itk-snap: An interactive tool for semi-automatic segmentation of multi-modality biomedical images," in *2016 38th annual international conference of the IEEE engineering in medicine and biology society (EMBC)*. IEEE, 2016, pp. 3342–3345.

[35] D. Knez, B. Likar, F. Pernuš, and T. Vrtovec, "Computer-assisted screw size and insertion trajectory planning for pedicle screw placement surgery," *IEEE Transactions on Medical Imaging*, vol. 35, no. 6, pp. 1420–1430, 2016.

[36] V. Vörös, R. Li, A. Davoodi, G. Wybaillie, E. Vander Poorten, and K. Niu, "An augmented reality-based interaction scheme for robotic pedicle screw placement," *Journal of Imaging*, vol. 8, no. 10, p. 273, 2022.

[37] M. Bakhtiarinejad, C. Gao, A. Farvardin, G. Zhu, Y. Wang, J. K. Oni, R. H. Taylor, and M. Armand, "A surgical robotic system for osteoporotic hip augmentation: System development and experimental evaluation," *IEEE Transactions on Medical Robotics and Bionics*, vol. 5, no. 1, pp. 18–29, 2023.

[38] T. N. Bernard Jr and C. E. Seibert, "Pedicle diameter determined by computed tomography. its relevance to pedicle screw fixation in the lumbar spine." *Spine*, vol. 17, no. 6 Suppl, pp. S160–3, 1992.

[39] A. Fedorov, R. Beichel, J. Kalpathy-Cramer, J. Finet, J.-C. Fillion-Robin, S. Pujol, C. Bauer, D. Jennings, F. Fennessy, M. Sonka *et al.*, "3d slicer as an image computing platform for the quantitative imaging network," *Magnetic resonance imaging*, vol. 30, no. 9, pp. 1323–1341, 2012.

[40] X. Chen, Q. Song, K. Wang, Z. Chen, Y. Han, H. Shen, and Q. Li, "Robot-assisted minimally invasive transforaminal lumbar interbody fusion versus open transforaminal lumbar interbody fusion: a retrospective matched-control analysis for clinical and quality-of-life outcomes," *Journal of Comparative Effectiveness Research*, vol. 10, no. 10, pp. 845–856, 2021.

[41] A. Chan, B. Coutts, E. Parent, and E. Lou, "Development and evaluation of ct-to-3d ultrasound image registration algorithm in vertebral phantoms for spine surgery," *Annals of Biomedical Engineering*, vol. 49, no. 1, pp. 310–321, 2021.

[42] P. Brößner, B. Hohlmann, K. Welle, and K. Radermacher, "Ultrasound-based registration for the computer-assisted navigated percutaneous scaphoid fixation," *IEEE Transactions on Ultrasonics, Ferroelectrics, and Frequency Control*, 2023.

[43] T.-H. Tsai, R.-D. Tzou, Y.-F. Su, C.-H. Wu, C.-Y. Tsai, and C.-L. Lin, "Pedicle screw placement accuracy of bone-mounted miniature robot system," *Medicine*, vol. 96, no. 3, 2017.

[44] B. Jiang, A. K. Ahmed, C. C. Zygourakis, S. Kalb, A. M. Zhu, J. Godzik, C. A. Molina, A. M. Blitz, A. Bydon, N. Crawford *et al.*, "Pedicle screw accuracy assessment in excelsiusgps® robotic spine surgery: evaluation of deviation from pre-planned trajectory," *Chinese neurosurgical journal*, vol. 4, no. 03, pp. 118–123, 2018.

[45] C. Gao, H. Phalen, A. Margalit, J. H. Ma, P.-C. Ku, M. Unberath, R. H. Taylor, A. Jain, and M. Armand, "Fluoroscopy-guided robotic system for transforaminal lumbar epidural injections," *IEEE Transactions on Medical Robotics and Bionics*, vol. 4, no. 4, pp. 901–909, 2022.